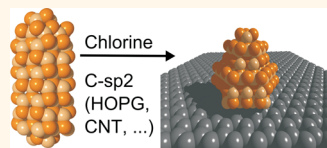


Interfacing Quantum Dots and Graphitic Surfaces with Chlorine Atomic Ligands

Fabiola Iacono,^{†,●} Cristina Palencia,^{‡,●} Leonor de la Cueva,[‡] Michaela Meyns,[§] Luigi Terracciano,[†] Antje Vollmer,[§] María José de la Mata,[†] Christian Klinke,[§] José M. Gallego,^{‡,§} Beatriz H. Juarez,^{‡,§,*} and Roberto Otero^{†,‡,*}

[†]Departamento de Física de la Materia Condensada and Instituto Nicolás Cabrera, Facultad de Ciencias, Universidad Autónoma de Madrid, UAM, Avd. Fco. Tomás y Valiente 7, 28049 Madrid, Spain, [‡]IMDEA Nanoscience, c/ Faraday 9, Campus de Cantoblanco, 28049 Madrid, Spain, [§]Institute of Physical Chemistry, University of Hamburg, Grindelallee 117, Hamburg, Germany, [§]Helmholtz Zentrum Berlin für Materialien und Energie GmbH, BESSY II, Albert-Einstein-Strasse 15, 12489 Berlin, Germany, [†]Servicio Interdepartamental de Investigación. Sldl. Universidad Autónoma de Madrid UAM, Avd. Fco. Tomás y Valiente 7, 28049 Madrid, Spain, [§]Instituto de Ciencia de Materiales de Madrid, ICMM, CSIC, Sor Ángela de la Cruz s/n, 28049 Madrid, Spain, and [§]Departamento de Química Física Aplicada, Facultad de Ciencias, Universidad Autónoma de Madrid UAM, Avd. Fco. Tomás y Valiente 7, 28049 Madrid, Spain. [●]Fabiola Iacono and Cristina Palencia have contributed equally to this work.

ABSTRACT The performance of devices based on semiconductor nanocrystals (NCs) improves both with stronger interface interactions among NCs and between NCs and solid electrode surfaces. The combination of X-ray photoelectron spectroscopy (XPS) and solid ³¹P CP/MAS NMR (cross-polarization/magic angle spinning nuclear magnetic resonance) shows that the selective substitution of long organic chains by chlorine atomic ligands during the colloidal synthesis by the hot injection method promotes the adsorption of CdSe NCs to carbon sp² surfaces, leading to the formation of well-ordered NC monolayers on graphitic materials.



KEYWORDS: CdSe nanocrystals · graphitic surface · graphene · atomic ligands · chlorine · interaction

Semiconductor nanocrystals (NCs) have found application as part of the active material in many optoelectronic and photovoltaic devices, due to their very interesting optical and electronic properties.¹ Usually, the performance of such devices is limited by the reduced charge mobility across the NC–NC and/or NC–electrode interfaces, because the surface of the colloidal NCs is stabilized by a shell of organic ligands that are usually long and poor electric conductors. The electronic mobility and thereby the performance of such devices can be enhanced by treatments that substitute the original insulating organic ligands for halides^{2,3} or inorganic shells,⁴ which improves the electronic NC–NC interface coupling.

Concerning the NC–electrode interface, a significant coupling has been reported for carbon C-sp² surface electrodes (carbon nanotubes (CNTs), graphene flakes, and graphitic surfaces covered with NCs).^{5–9} These systems have been studied mainly because of their photoconductive response as a result of the possible photoinduced electron transfer across

the interface upon optical excitation. Furthermore, for many applications, it is important to preserve the electronic transport properties across the C-sp² lattice. This implies that the interface should not be modified by covalent functionalization. One way to obtain noncovalently functionalized C-sp² lattices decorated with CdSe NCs is by adding 1,2-dichloroethane (DCE) during the synthesis of rodlike CdSe NCs by hot injection in the presence of such C-sp² surfaces.⁹ Whether this method leads to chlorine incorporation in the ligand shell, the way in which the halogen could get incorporated to that shell, or the effect that this incorporation could have in mediating the interaction with the surface are questions which remain unexplored. It has been recently reported that molecular chlorine interacts with Se surface atoms of PbSe NCs passivating the surface, and preventing oxidation¹¹ and chloride ions decisively modifies the growth of branched NCs.¹² Chlorine ligand exchange has been followed by ¹H and ³¹P NMR spectroscopy¹³ and the coupling of nuclear magnetic resonance (NMR) and X-ray photoelectron

* Address correspondence to roberto.oteru@uam.es.

Received for review December 19, 2012 and accepted February 8, 2013.

Published online February 08, 2013
10.1021/nn305868n

© 2013 American Chemical Society

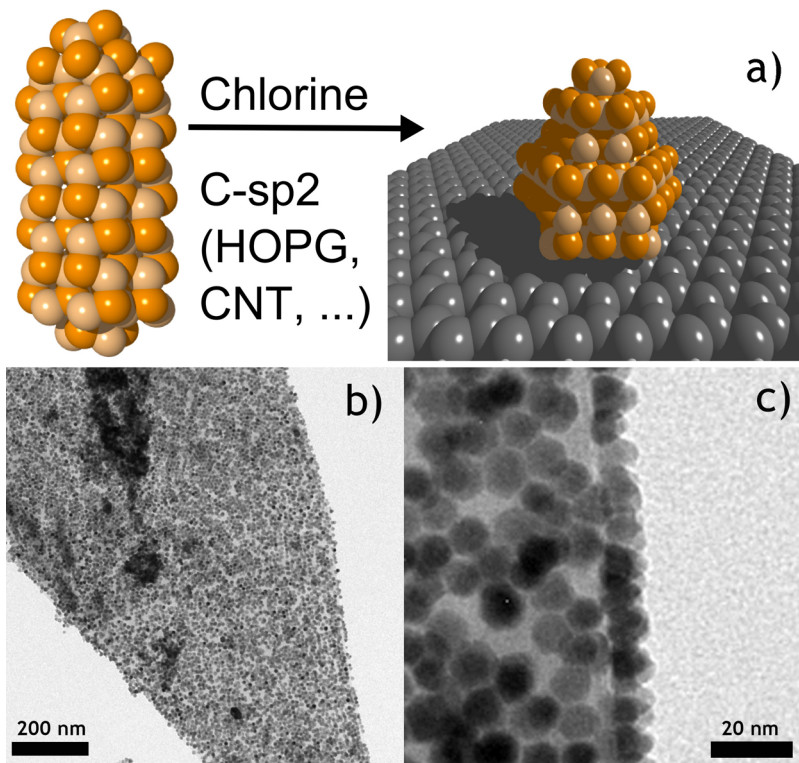


Figure 1. (a) Sketch of a CdSe rod that in the presence of 1,2-dichloroethane modifies its shape and self-assemblies on C-sp² surfaces. (b,c) TEM images of CdSe nanoparticles grown on HOPG flakes at different magnifications.

spectroscopy (XPS) has proven to be a powerful tool to successfully elucidate the surface and the interface in core–shell structures.¹⁴

In this paper we demonstrate by XPS and solid NMR that Cl is incorporated in the ligand shell of NCs decorating C-sp² surfaces; that such incorporation involves the selective substitution of anhydrides of ODPA in the organic capping shell (originally composed of ODPA²⁻ and anhydrides of ODPA); and finally that the structural changes associated with the aforementioned substitution actually strengthen the interaction of the NCs with C-sp² surfaces. These investigations have been carried out on highly-oriented pyrolytic graphite (HOPG), as a model system for general C-sp² surfaces such as CNTs or graphene.^{9,10} This one-pot methodology leads to long-range ordered NC monolayers with a close contact between the active NC layer and the C-sp² electrode surface. The possibility to control the coverage of hexagonal ordered NC monolayers on conductive C-sp² in one pot opens attractive alternatives to be explored in solution processed optoelectronics.

RESULTS AND DISCUSSION

To clarify the role of chlorine it is worth keeping in mind that the addition of chlorinated cosolvents such as DCE not only promotes the adsorption of NCs to carbonaceous surfaces but also leads to a reshaping of the NCs, from rodlike shape in the absence of chlorine, to dihexagonal pyramids⁹ in its presence. Figure 1a schematically depicts these processes, where the Cd

(000–1) planes are epitaxially matched to the outer C-sp² surface.¹⁵ Figure 1 panels b and c show transmission electron microscope (TEM) images of CdSe NCs covering homogeneously the surface of HOPG flakes at different magnifications (see methods for synthetic details and Supporting Information, Figure S1 for SEM images of flakes at different magnifications).

In Figure 2, SEM images of HOPG surfaces covered with pyramidal CdSe NCs grown in the presence of DCE are shown (more images can be found in Supporting Information, Figure S2). The surfaces show different coverage, determined as the fraction of area covered by NCs in the images. A similar self-organization as that obtained for graphite flakes in Figure 1 can be observed. While samples exhibiting high coverage (Figure 2a) show small uncovered areas sparsely distributed, in low covered substrates (Figures 2c,d), the NCs mostly arrange either in small islands or individually. NCs average sizes vary from 13.0 ± 1.3 nm (Figure 2a), 12.7 ± 1.5 nm (Figure 2b), 6.2 ± 0.8 nm (Figure 2c), and 9.9 ± 1.0 nm (Figure 2d). The standard deviation has been calculated from *ca.* 50 statistical measurements from TEM images. Different sizes might lead to different interaction strengths between the NC and the surface and thus to higher coverage for samples with larger NCs. We ascertained that such a correlation, however, does not exist. Moreover, since samples exhibiting a bimodal size distribution show equal coverage for the different size modes (see Figure S3 in the Supporting Information), we discard the differences

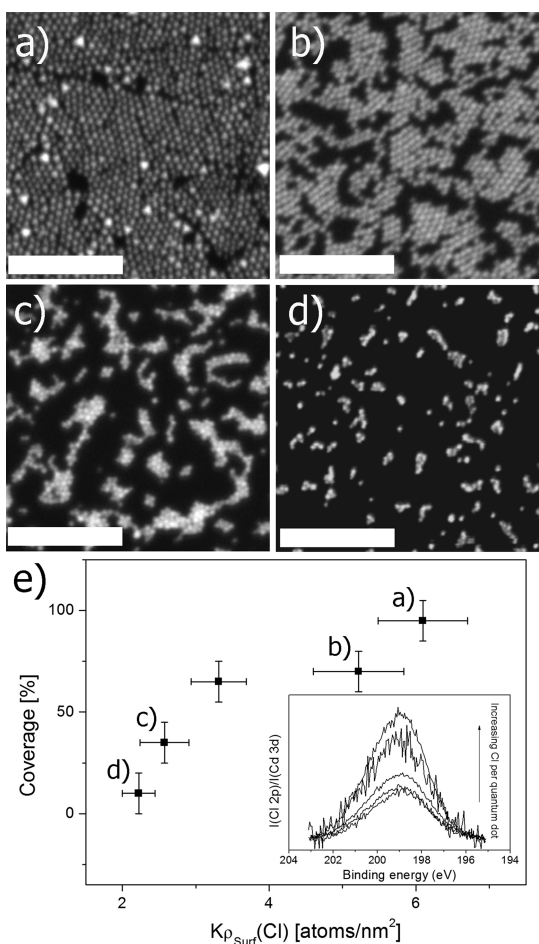


Figure 2. (a–d) SEM images of pyramidal CdSe NCs grown on HOPG surfaces with different coverage. Scale bar: 300 nm. The labels correspond to the plotted points in the lower panel, showing the coverage (in percent) *versus* the relative quantity of Cl per nanoparticle (see text and Methods). The inset shows the Cl region XPS spectra of the samples normalized to the quantity of Cd and multiply to the mean radius r of the NCs for each sample. $h\nu = 1486.61$ eV and energy pass = 50 eV.

in size as a parameter decisively contributing to the observed coverage tendency.

Another factor which might likely control the interaction across the C-sp²/NC interface and, thus, the coverage degree, is the chemical composition of the NC surface. To explore this possibility we have carried out systematic XPS experiments in samples showing different coverage. Actually, the samples shown in Figure 2a–d are suitable for such experiments, as the arrangement of similar NCs on conductive substrates and in a single layer helps avoiding charging effects. All the spectra recorded for samples synthesized in the presence of DCE display a measurable Cl 2p peak (inset Figure 2e) centered at about 199 eV. This is in good agreement with the binding energy of the Cl 2p core level in CdCl₂ and previously reported values for atomic Cl-terminated CdSe NCs.¹⁸ To obtain a meaningful measure of the amount of chlorine *per* NC, we have normalized all the spectra to the Cd signal, taking into

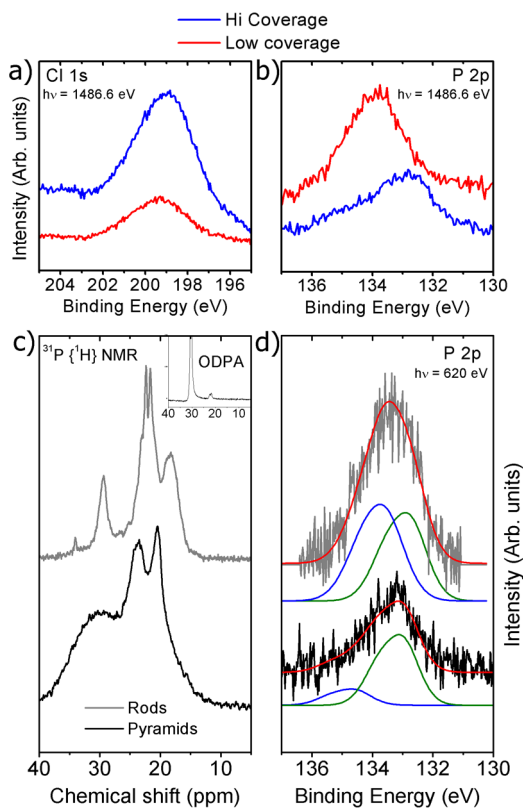


Figure 3. (a,b) HR XPS signals of samples exhibiting low coverage of NCs (red line) and high coverage (blue line): (a) Cl 2p and (b) P 2p regions. (c) Solid ³¹P{¹H} NMR of rodlike (upper gray line) and pyramidal CdSe NCs (lower black line). Inset: pure ODPA. (d) P 2p region acquired for rodlike (upper gray line) and pyramidal NCs (lower black line) by XPS ($h\nu = 620$ eV) The P 2p peaks can be deconvoluted in two components with different binding energies (green and blue lines for ODPA²⁻ and anhydrides respectively, see text).

account the mean radius (r) of the NCs, as described in Methods. The results are shown in the plot (Figure 2e) for the samples whose coverage was previously characterized by SEM. The error bars in the y-axis correspond to $\pm 10\%$ in the coverage values obtained from the SEM images. The error bars in the x-axis correspond to values including (r) according to the standard deviation. This plot shows that the resulting coverage for similar growth conditions increases with increasing the surface concentration of Cl on the NCs, indicating that the interaction between the NCs and the C-sp² surface is stronger for NCs with high amounts of Cl on the surface. Notice that if the measured signal of chlorine arose from chlorine adsorbed on the C-sp² surface instead of to the NCs surface, we would expect a higher Cl/Cd ratio for samples with a low NCs coverage, contrary to our observations.

Thus, it is clear that Cl incorporation must have an effect on the ODPA-related ligand shell. Since phosphorus is only present in the ligand molecules, XPS of the P and the Cl signals will provide information about the influence of Cl in the ligand shell. Figure 3 panels a and b show XPS spectra of both P and Cl performed on

samples exhibiting high and low coverage. For comparison, all the spectra have been normalized to the amount of Cd, as in Figure 2. We observe that, with respect to the low coverage samples, the P 2p signal (area under the curve) for samples exhibiting high coverage decreases roughly in the same proportion that the Cl signal increases, pointing toward a substitutional incorporation of chlorine in the ligand shell against the phosphorus-containing ligands. It is worth mentioning that not only the intensity of the signal, but also the shape and peak position are modified by the presence of chlorine. This result indicates that there are different chemical environments for P and that not all of them are equally affected by the presence of the halogen.

To investigate the chemical changes on the P sites, comparative studies have been carried out on samples synthesized in the absence of chlorinated cosolvents (what yields rodlike shape NCs) and samples showing a high concentration of chlorine on the surface (pyramidal shape) by solid ^{31}P NMR. Previous solution ^{31}P NMR characterizations of CdSe NCs synthesized in the presence of mixtures of octadecylphosphonic acid (ODPA), trioctylphosphine (TOP), and trioctylphosphine oxide (TOPO) have shown that the organic shell is mainly composed of phosphonic acid-related species bonded to the surface Cd atoms^{16,17} in the form of phosphonates.¹⁸ Moreover, quantitative NMR studies have identified that the shell of CdSe rodlike NCs is composed of a mixture of ODPA anhydrides and the single deprotonated ODPA specie (octadecyl hydrogen phosphonate, ODPA⁻) in a 45/55 mass ratio.¹⁹ Other authors rather claim that the shell is a mixture of the double deprotonated specie (octadecylphosphonate (ODPA²⁻) and anhydrides.²⁰

To avoid the acidic digestion of the inorganic NCs for the liquid characterization of the ligands, in this work solid ^{31}P NMR spectroscopy²¹⁻²³ has been performed instead. Figure 3c shows the solid $^{31}\text{P}\{^1\text{H}\}$ NMR spectra for rodlike CdSe NCs (upper line) and dihexagonal pyramids (lower line), respectively (not supported on the C- sp^2 surface, see Methods for further details). Previously reported solution ^{31}P NMR spectra of ODPA-capped CdSe NCs consisted of two broad signals centered at 20 and 30 ppm.^{19,24} The solid spectra shown in Figure 3c show distinct sets of well-defined signals both for rodlike and pyramidal NCs. Comparison between them reveals that the transformation from rod to pyramids involves a shift and/or broadening of the signals. This indicates a different chemical environment for P in rodlike and pyramidal NCs, and might thus be interpreted as a fingerprint for the incorporation of chlorine in the ligand shell.

The remarkable resolution in the solid $^{31}\text{P}\{^1\text{H}\}$ NMR spectra shown in Figure 3c enables the assignment of the signals to different chemical environments for P. We believe this resolution is related to the size of the NCs showing relatively large crystallographic facets

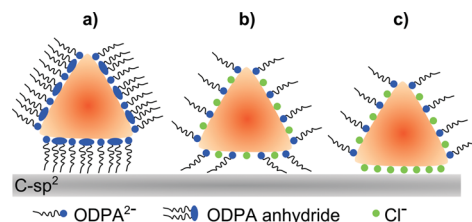
and allowing for a high structural order of the surface. In particular, the $^{31}\text{P}\{^1\text{H}\}$ NMR spectrum of rodlike NCs (Figure 3c, upper line) shows a peak at 18.3 ppm; a prominent signal around 22–23 ppm terminated in two narrow peaks at 21.7 and 22.4 ppm; and two additional signals at 29.3 and 34.0 ppm. The absence of peaks at higher chemical shifts (>35 ppm) discards the presence of TOPO bonded to the NC surface, in agreement with previous studies.¹⁶ Three of such signals (29.3, 22.4, and 21.7 ppm) can also be found in the solid $^{31}\text{P}\{^1\text{H}\}$ NMR spectrum of pure ODPA (see inset). The dominating contribution at 30.4 ppm is similar to the value reported for solution ODPA ^{31}P NMR.^{16,17} The signals observed in Figure 3c at ~22 ppm and 18.3 ppm can be assigned to ODPA species directly bound to Cd in the form of octadecylphosphonates (double deprotonated ODPA²⁻) and anhydrides of phosphonic acids, respectively.^{19,20,23,24} The presence of ODPA (neutral molecule) could be related with the hydrolysis of anhydrides and hydrogen bonding between ODPA molecules might be the origin of the peaks at 22.4 and 21.7 ppm, according to previous work.¹⁷ Finally, we attribute the small signal at 34 ppm to a small contribution of Se-TOP. Thus, out of all the contributions found in the solid ^{31}P NMR spectra, the two main components that can be unambiguously attributed to species in the ligand shell are those corresponding to ODPA²⁻ and ODPA anhydrides.

For pyramidal NCs (Figure 3c, lower line), the peaks previously assigned to ODPA²⁻ and ODPA anhydrides are slightly shifted downfield when compared to the spectrum of rodlike NCs. Furthermore, a slight downfield shift is also observed by solid state ^1H MAS NMR experiments in the pyramidal NCs compared to rodlike (see Figure S4 Supporting Information). The shift in the whole spectrum could be attributed to the influence of adjacent chlorine atoms in the shell. Alternatively, this shift may be related to a slightly different binding against the predominant (1–101) polar facets terminated in Cd in the case of pyramids^{9,15} compared to the predominant nonpolar (01–10) facets in rods. The range between 25 and 40 ppm shows a broad undefined peak, and the two contributions at 21.7 and 22.4 ppm are not observed, which may indicate breaking of the hydrogen bonds in the presence of chlorine. Typically, the ^{31}P NMR signals of phosphonic acid chlorides are shifted 14 to 20 ppm downfield from the corresponding phosphonic acids.²⁵ Thus, the relatively small chemical shift observed in Figure 3 discards the halogen substitution within the ODPA molecule (*i.e.*, –P-Cl bound).

Changes in the P core levels of the NCs are also apparent in synchrotron XPS. Figure 3d shows the P 2p region acquired for rodlike and pyramidal NCs, respectively. Notice that the shape of the peak for rodlike NCs is similar to that shown in Figure 3b for low coverage samples, and very different from the spectra for Cl-rich NCs.

This indicates that the progressive incorporation of chlorine leads to a continuous transformation of the P 2p peak shape from a symmetrical signal for Cl-poor to an asymmetric one for Cl-rich NCs. The natural line shape for 2p levels is that of an asymmetric spin-split doublet, very different from the line shape found for Cl-poor NCs. Such symmetric appearance can be well reproduced by assuming two different and equally populated chemical environments for P at the surface of the rods, leading to two components with similar intensities in the XPS signal, but different binding energies (132.92 and 133.74 eV, respectively, for the spectrum in Figure 3d upper line). The shape of the XPS signal for Cl-rich NCs is however much more asymmetric and, thus, more consistent with a single environment of P on their surface. If two components are still allowed for fitting the experimental data, it is found that the intensity of the highest-binding energy one is now much smaller than in Cl-poor samples (compared to the intensity of the low-binding energy component), and both components have been shifted to higher binding energies (133.11 and 134.71 eV respectively for the spectrum in Figure 3d, lower line). This small shift of about 0.1 eV for both components follows the same trend of the downfield-shifted signals observed in the NMR spectrum upon chlorine incorporation. Furthermore, the width of the P 2p signal for anhydrides is slightly larger (1.24 eV) than that related to the ODPA^{2-} molecules (1.11 eV), which may be related to the variable phosphorus environment in anhydrides of different chain length.

The fact that two main components are observed for the phosphorus signals related to ligand shell species both in XPS and NMR suggests identification between them. We attribute the signal at the lowest binding energy to ODPA^{2-} in agreement with previous results²⁰ and the signal at higher binding energy to anhydrides of ODPA. To evaluate the adsorption of the ligand molecules on the Cd rich (000-1) crystal facet of CdSe in terms of adsorption geometry, adsorption energy, and partial charge on the atoms we performed simulations using DFT in the frame of the ORCA software.²⁶ To reduce computing time, the simulated alkyl chains of the ODPA species contain 3 carbon atoms instead of 18, which does not affect the qualitative conclusions. We used the LDA exchange functional, the correlation functional VWN5,²⁷ and the Ahlrichs TZV basis set.²⁸ The partial charge on the atoms was calculated by the Loewdin method. The adsorption energy was calculated by comparison of the sum of the energies of the CdSe crystal and the ligand molecule as separated moieties, and the total energy of the combined, optimized system, in which the crystal geometry was kept fixed at the experimental values and the ligand molecule was free to relax. The results of these simulations state the partial charge on P atoms in the ODPA^{2-} molecule is 1.64 e and the adsorption energy amounts to 11.4 eV. The partial



Scheme 1. The incorporation of chlorine (green dots) in the original ODPA-related ligand shell promotes the interaction with carbon sp^2 surfaces. (a) The original shell combines ODPA^{2-} and anhydrides; (b) the presence of chlorine displaces the anhydrides selectively and (c) promotes the interaction with C-sp^2 surfaces.

charge on P atoms of the anhydrides, simulated as the condensation product of 2 units of ODPA and twice deprotonated equals 1.66 e and the corresponding adsorption energy is 10.4 eV. These DFT calculations of adsorbed ODPA^{2-} and anhydrides on the CdSe surface show that phosphorus atoms in the anhydride environment are slightly more positive than in the ODPA^{2-} molecule and thus, a higher binding energy for the anhydride species in the XPS core levels might be expected.

Notice that, with this interpretation, the transformation from Cl-poor to Cl-rich samples is associated with a very important decrease in anhydrides of ODPA, while the amount of more strongly bound ODPA^{2-} remains mostly unperturbed. This also implies a reduction of the total amount of phosphorus in Cl-rich samples, in good agreement with the results of Figure 3b and supported by inductively coupled plasma optical emission spectrometry (ICP-OES), where the Cd/P ratios are larger for pyramidal NCs produced in the presence of chlorine than those obtained for rodlike NCs (see Methods). The proposed modification of the ligand shell supports the selective elimination of the long alkyl-chain ligands (anhydrides of ODPA) and favors a closer contact between the NCs and the carbon surface, as depicted in Scheme 1. This fact is in agreement with previous high-resolution transmission electron microscopy (HRTEM) investigations where lateral distances in between NCs attached to CNTs were easily observable while no observable distance between NCs and the CNTs discarded the presence of the original ODPA capping ligands on the (000-1) Cd-rich facet.⁹ Furthermore, the Cl ligand might contribute to the strengthening of the electrostatic interaction with the polarizable C-sp^2 lattice.

CONCLUSIONS

We have shown that the addition of a chlorinated cosolvent to the reaction media of CdSe rodlike NCs leads to the incorporation of chlorine as atomic ligands by selective substitution of anhydrides of octadecylphosphonic acid, while octadecylphosphonates remain anchored to the surface of the NC. Such substitution modifies the structure of the ligand shell, reducing the density of long-chain organic ligands, thus allowing a closer contact at the interface between

HOPG and CdSe NCs. This incorporation strengthens the interaction, as demonstrated by the fact that NCs with larger amounts of chlorine on their surface (determined by XPS) decorate the C-sp² surfaces more efficiently than particles with a lower amount. We expect such an effect to take place also for other combinations of semiconductor NCs and solid surfaces, which might be relevant for electrode—semiconductor

NC interfaces where control of the optical dynamics of interacting objects could drive favorable coupling mechanisms. Finally, we believe that the possibility to fabricate well-covered carbon-sp² electrodes (carbon nanotubes, graphene, highly oriented pyrolytic graphite, ...) with semiconductor NCs in one pot by means of the hot injection is, undoubtedly, an attractive issue for solution processed optoelectronics.

METHODS

Chemicals. CdO (99.99%) and trioctylphosphine technical grade (TOP) were purchased from Sigma Aldrich. Trioctylphosphine oxide (TOPO) was purchased from Merck and octadecylphosphonic acid (ODPA) from Alfa Aesar. Methanol, toluene, and 1,2-dichloroethane (DCE) were purchased from Panreac. Highly oriented pyrolytic graphite (HOPG) substrates, ZYB quality, piece sizes of 1 cm² and thickness of 2 mm were purchased from NT-MDT. CdSe powder of 10 μm particle size, 99.99% trace metal basis electronic grade (244600), was purchased from Sigma Aldrich.

Synthesis of Rodlike and Pyramidal CdSe Nanocrystals on HOPG. CdSe nanocrystals on HOPG substrates were grown following reported recipes^{9,10} with some variations. HOPG substrates were included in the reaction flask together with the magnetic stirrer. As a consequence of the stirring, some flakes can be peeled off from the HOPG. Since they contain several graphene layers, they can be inspected by TEM (Figure 1). In a typical procedure, 0.025 g of CdO were complexed with 0.20 g of ODPA at 280 °C in the presence of 2.9 g of TOPO (under N₂). Once a clear solution is obtained the temperature of the reaction mixture was decreased and kept at 85 °C for 30 min. To obtain pyramidal NCs, volumes of 1,2-dichloroethane ranging from 3.0 to 4.5 μL were injected with the help of a Hamilton microsyringe (701SN 10 μL total volume with a 11 cm needle to ensure reaching the level of the solution). For rodlike nanocrystals, no DCE was added. The temperature was further raised to 265 °C, and 0.42 mL of Se dissolved in TOP (1 M) was injected. The temperature was kept to 255 °C for 21 h and quenched by decreasing the temperature to 70 °C and adding toluene (3 mL). Once the reaction was finished, HOPG substrates were separated from the reaction media and washed several times by immersion in several toluene baths. They were dried in air and kept afterward in N₂. The remaining NCs (not attached to HOPG substrates) were washed in several cycles of centrifugation (upon the addition of methanol) and manual shaking (in toluene). The washed CdSe NCs were dispersed in toluene and maintained in the dark at 4 °C. As described in the main text, some flakes can be inspected by TEM due to the peeling from the HOPG substrate during the reaction (see Supporting Information for SEM images at different magnifications).

Transmission Electron Microscopy. TEM has been performed on a JEOL 1010 with an acceleration voltage of 100 keV. The scanning electron microscopy images were acquired in a field emission microscope (FE-SEM) Philips XL30 S-FEG and in a FEI microscope Nova Nanosem 230 model.

Solid ¹H MAS and ³¹P CP/MAS NMR Experiments. ¹H MAS and ³¹P CP/MAS solid state NMR (cross-polarization/magic angle spinning nuclear magnetic resonance) spectra were collected at room temperature on a Bruker AV 400 WB spectrometer equipped with 4 mm and 2.5 mm MAS probes. For that, all the samples were prepared by centrifugation and drying of NCs dispersions. Note that all NMR experiments have been performed over CdSe NCs (both, rodlike and pyramidal shaped, without the presence of the sp² carbon substrates). The obtained sediments were transferred either to a 4 mm or to 2.5 mm diameter probes. For the 2.5 mm probe ³¹P CP/MAS experiments, an excitation 1H $\pi/2$, 2.2 μ s pulse was used with 50 kHz spectral width, 4 ms contact time, and high power proton decoupling tppm15 at 115 kHz. Recycled delay was set at 5 s.

For the 4 mm probe experiments, an excitation 1H $\pi/2$, 3 μ s pulse was used with 35 kHz spectral width, 2 ms contact time and high power proton decoupling tppm15 at 80 kHz. Recycled delay was set at 5 s. All spectra were referenced to 85% phosphoric acid (0 ppm) as standard. The solid ³¹P CP/MAS NMR spectrum of ODPA was acquired by direct measurement of the purchased product. High spinning speed hinders polarization transfer from ¹H to ³¹P but, at the same time, it is necessary to obtain better resolution, so the experimental conditions were optimized to balance these effects. The spectrum of rodlike CdSe NC was recorded at a spinning speed of 7 kHz, while it was necessary to increase the spinning speed up to 30 kHz to obtain well resolved peaks in the case of pyramidal CdSe NCs.

Inductively Coupled Plasma Optical Emission Spectrometry (ICP-OES). ICP-OES was performed in a PerkinElmer Optima 2100 DV. For this purpose samples were digested with aqua regia (nitric acid and hydrochloric acid mixture 1/3 v/v) to dissolve the particles and further diluted. Cd/Se molar ratios are in all cases close to unity within experimental error. For rodlike NCs produced after 21 h, molar ratio Cd/P is at least 3 times lower than those obtained for pyramidal NCs, indicating a lower concentration of P for pyramidal NCs.

X-ray Photoelectron Spectroscopy. Samples of NCs attached to HOPG were fixed with tantalum foils to the samples holders and inserted in a prevacuum chamber, prior to the XPS measurements. X-ray photoelectron spectroscopy has been performed in two different experimental setups, one at our laboratory and another at the Helmholtz Zentrum Berlin für Materialien und Energie GmbH, BESSY II with different photon energies. While the main features observed in the obtained spectra are independent of the photon energy, we found that our laboratory Al-K α source ($h\nu = 1486$ eV) was not well suited for the study of the P 2p signal, since in this energy region a rather strong overlap is found with the LMM Se Auger peak. Synchrotron experiments with a photon energy of $h\nu = 620$ eV allow a direct observation of the P 2p peak unperturbed by any other spectral components.

Normalized Cl/Cd Values. The XPS intensity of a given element A is proportional to the total amount of this element inside the X-ray beam spot. This amount is the product of the total number of NCs within the beam spot (N) times the amount of the element in each NC, which we will denote $[A]$. If the element A is distributed all over the NC's bulk with a density $\rho_{\text{bulk}}(A)$ (in atoms per unit volume), and assuming nearly spherical NCs of radius R , $[A]$ will be given by $\rho_{\text{bulk}}(A) \cdot 4\pi R^3/3$. On the other hand, if element A is confined to the surface of the NC with a surface density $\rho_{\text{surf}}(A)$ (in atoms per unit surface) and the same assumption about the NC shape as before, then $[A]$ will take the value $\rho_{\text{surf}}(A) \cdot 4\pi R^2$. Thus, if we have an element A distributed in the bulk of the NC and another element B distributed only at the surface, the ratio between the intensities of B and A will be given by $I(B)/I(A) \sim (\rho_{\text{surf}}(B)) / (\rho_{\text{bulk}}(A)R)$. Therefore, the quantity $\rho_{\text{bulk}}(A) \cdot I(B)/I(A)$ equals the surface density of B at each NC except for a dimensionless proportionality constant, $K\rho_{\text{surf}}(B)$. In our case we are interested in measuring the different amounts of Cl at the NC surfaces, and we use the Cd signal as the bulk normalizing element, with $\rho_{\text{bulk}}(\text{Cd}) = 1.83 \times 10^{22}$ atoms/cm³.

Conflict of Interest: The authors declare no competing financial interest.

Supporting Information Available: Figure S1 shows SEM images of HOPG flakes covered with CdSe NCs isolated from

the synthesis. Figure S2 shows SEM images of differently covered HOPG surfaces at different magnifications. Figure S3 shows SEM images of NCs attached to HOPG showing two clear distinct NCs size populations. Figure S4 is the solid ¹H NMR spectra for rodlike and pyramidal NCs. This material is available free of charge via the Internet at <http://pubs.acs.org>.

Acknowledgment. B.H.J. thanks the European Commission for FP7-PEOPLE-ERG-2008 (239256), the former Spanish Ministry of Science and Innovation for RYC-2007-01709 and MAT-2009-13488. C.K. and M.M. acknowledge the Deutsche Forschungsgemeinschaft (DFG) for financial support. Financial support from the Ministerio de Ciencia e Innovación (FIS2010-18847, FIS2012-33011 and Consolider-Ingenio en Nanociencia Molecular, ref CSD2007-00010), Comunidad de Madrid (Grant S2009/MAT-1726) and EU (SMALL, PITN-GA-2009-23884) is gratefully acknowledged. The authors thank Dr. Emilio Pérez for fruitful discussions.

REFERENCES AND NOTES

1. Huynh, W. U.; Dittmer, J. J.; Alivisatos, A. P. Hybrid Nanorod-Polymer Solar Cells. *Science* **2002**, *295*, 2425–2427.
2. Tang, J.; Kemp, K. W.; Hoogland, S.; Jeong, K. S.; Liu, H.; Levina, L.; Furukawa, M.; Wang, X.; Debnath, R.; Cha, D.; et al. Colloidal-Quantum-Dot Photovoltaics Using Atomic-ligand Passivation. *Nat. Mater.* **2011**, *10*, 765–771.
3. MacDonald, B. I.; Martucci, A.; Rubanov, S.; Watkins, S. E.; Mulvaney, P.; Jasieniak, J. J. Layer-by-Layer Assembly of Sintered CdSe_(x)Te_{1-x} Nanocrystal Solar Cells. *ACS Nano* **2012**, *6*, 5995–6004.
4. Lee, J. S.; Kovalenko, M. V.; Huang, J.; Chung, D. S.; Talapin, D. V. Band-Like Transport, High Electron Mobility and High Photoconductivity in All-Inorganic Nanocrystal Arrays. *Nat. Nanotechnol.* **2011**, *6*, 348–352.
5. Kamat, P. V. Quantum Dot Solar Cells. Semiconductor Nanocrystals as Light Harvesters. *J. Phys. Chem. C* **2008**, *112*, 18737–18753.
6. Konstantatos, G.; Badioli, M.; Gaudreau, L.; Osmond, J.; Bernechea, M.; Pelayo García de Arquer, F.; Gatti, F.; Koppens, F. H. L. Hybrid Graphene–Quantum Dot Phototransistors with Ultrahigh Gain. *Nat. Nanotechnol.* **2012**, *7*, 363–368.
7. Li, X.; Jia, Y.; Cao, A. Tailored Single-Walled Carbon Nanotube–CdS Nanoparticle Hybrids for Tunable Optoelectronic Devices. *ACS Nano* **2010**, *4*, 506–512.
8. Chanaewa, A.; Juarez, B. H.; Weller, H.; Klinke, C. Oxygen and Light Sensitive Field-Effect Transistors Based on ZnO Nanoparticles Attached to Individual Double-Walled Carbon Nanotubes. *Nanoscale* **2012**, *4*, 251–256.
9. Juarez, B. H.; Klinke, C.; Kornowski, A.; Weller, H. Quantum Dot Attachment and Morphology Control by Carbon Nanotubes. *Nano Lett.* **2007**, *7*, 3564–3568.
10. Juarez, B. H.; Meyns, M.; Chanaewa, A.; Cai, Y.; Klinke, C.; Weller, H. Carbon Supported CdSe Nanocrystals. *J. Am. Chem. Soc.* **2008**, *130*, 15282–15284.
11. Bae, W. K.; Joo, J.; Padilha, L. A.; Won, J.; Lee, D. C.; Lin, Q.; Koh, W. K.; Luo, H.; Klimov, V. I.; Pietryga, J. M. Highly Effective Surface Passivation of PbSe Quantum Dots Through Reaction with Molecular Chlorine. *J. Am. Chem. Soc.* **2012**, *134*, 20160–20168.
12. Kim, M. R.; Miszta, K.; Povia, M.; Brescia, R.; Christodoulou, S.; Prato, M.; Marras, S.; Manna, L. Influence of Chloride Ions on the Synthesis of Colloidal Branched CdSe/CdS Nanocrystals by Seeded Growth. *ACS Nano* **2012**, *6*, 11088–11096.
13. Anderson, N. C.; Owen, J. S. Soluble, Chloride-Terminated Cadmium Selenide Nanocrystals: Ligand Exchange Monitored by ¹H and ³¹P NMR Spectroscopy. *Chem. Mater.* **2013**, *25*, 69–76.
14. Virieux, H.; Le Troedec, M.; Cros-Gagnieux, A.; Ojo, W. S.; Delpech, F.; Nayral, C.; Martinez, H.; Chaudret, B. InP/ZnS Nanocrystals: Coupling NMR and XPS for Fine Surface and Interface Description. *J. Am. Chem. Soc.* **2012**, *134*, 19701–19708.
15. Hungria, A. B.; Juarez, B. H.; Klinke, C.; Weller, H.; Midgley, P. A. 3-D Characterization of CdSe Nanoparticles Attached to Carbon Nanotubes. *Nano Res.* **2008**, *1*, 89–97.
16. Peng, Z. A.; Peng, X. Nearly Monodisperse and Shape-Controlled CdSe Nanocrystals via Alternative Routes: Nucleation and Growth. *J. Am. Chem. Soc.* **2002**, *124*, 3343–3353.
17. Liu, H.; Owen, J. S.; Alivisatos, A. P. Mechanistic Study of Precursor Evolution in Colloidal Group II–VI Semiconductor Nanocrystal Synthesis. *J. Am. Chem. Soc.* **2007**, *129*, 305–312.
18. Owen, J. S.; Park, J.; Trudeau, P. E.; Alivisatos, A. P. Reaction Chemistry and Ligand Exchange at Cadmium–Selenide Nanocrystal Surfaces. *J. Am. Chem. Soc.* **2008**, *130*, 12279–12281.
19. Gomes, R.; Hassinen, A.; Szczygiel, A.; Zhao, Q.; Vantomme, A.; Martins, J. C.; Hens, Z. Binding of Phosphonic Acids to CdSe Quantum Dots: A Solution NMR Study. *J. Phys. Chem. Lett.* **2011**, *2*, 145–152.
20. Morris-Cohen, A. J.; Donakowski, M. D.; Knowles, K. E.; Weiss, E. A. The Effect of a Common Purification Procedure on the Chemical Composition of the Surfaces of CdSe Quantum Dots Synthesized with Trioctylphosphine Oxide. *J. Phys. Chem. C* **2010**, *114*, 897–906.
21. Bucera, L. R.; Murray, C. B.; Griffin, R. G.; Bawendi, M. G. Investigation of the Surface Morphology of Capped CdSe Nanocrystallites by ³¹P Nuclear Magnetic Resonance. *J. Chem. Phys.* **1994**, *100*, 3297–3300.
22. Ratcliffe, C. I.; Yu, K.; Ripmeester, J. A.; Zaman, M. B.; Badarau, C.; Singh, S. Solid State NMR Studies of Photoluminescent Cadmium Chalcogenide Nanoparticles. *Phys. Chem. Chem. Phys.* **2006**, *8*, 3510–3519.
23. Kopping, J. T.; Patten, T. E. Identification of Acidic Phosphorus-Containing Ligands Involved in the Surface Chemistry of CdSe Nanoparticles Prepared in Tri-N-Octylphosphine Oxide Solvents. *J. Am. Chem. Soc.* **2008**, *130*, 5689–5698.
24. Ohms, G.; Grossmann, G.; Schwab, B. Synthesis and ³¹P and ¹³C NMR Studies of Pyrophosphonic Acids. *Phosphorus, Sulfur Silicon Relat.* **1992**, *68*, 77–89.
25. Rogers, R. S. A General Synthesis of Phosphonic Acid Dichlorides Using Oxalyl Chloride and DMF Catalysis. *Tetrahedron Lett.* **1992**, *33*, 7473–7474.
26. Neese, F. The ORCA program system. *Wiley Interdiscip Rev.: Comput. Mol. Sci.* **2012**, *2*, 73–78, <http://www.thch.uni-bonn.de/tc/orca/>.
27. Vosko, S. H.; Wilk, L.; Nusair, M. Accurate Spin-dependent Electron Liquid Correlation Energies for Local Spin Density Calculations: a Critical Analysis. *Can. J. Phys.* **1980**, *59*, 1200–1211.
28. Schäfer, A.; Horn, H.; Ahlrichs, R. Fully Optimized Contracted Gaussian Basis Sets for Atoms Li to Kr. *J. Chem. Phys.* **1992**, *97*, 2571–2577.